

## Schematic suggestion of two-layer coating system for controlling corrosional toxicity of titanium dioxide from dental implant fixture

Bonzoon Goo<sup>1,2</sup>, Tomáš Navrátil<sup>1</sup>, Ivan Matouš Malbohan<sup>1</sup>

<sup>1</sup>Institute of Medical Biochemistry and Laboratory Diagnostics, First Faculty of Medicine, Charles University and General University Hospital in Prague, Prague, Czech Republic,

<sup>2</sup>Department of Prosthodontics, Dental Goo Hospital, Daejeon, Republic of Korea

\*Correspondence: Bonzoon Goo; [bonzoon@seznam.cz](mailto:bonzoon@seznam.cz); Tel.: +420723240886, +82422555218, FAX: +42022496284

 <https://orcid.org/0000-0002-9568-0779>

### Abstract

#### Introduction

Titanium dioxide has been classified by the International Agency for Research on Cancer (IARC) as a Group 2B carcinogen. As indispensable material for dental implant fixture, dental patients are exposed to its toxicological reactions.

#### Objectives

The primary aim of this research is to prevent making nanoparticle titanium dioxide from the corrosion of dental implant fixture.

#### Methods

The authors introduce two-layer coating system for controlling corrosional toxicity of TiO<sub>2</sub> from the surface of two dental implant fixtures by medronic acid and teriparatide acetate.

#### Results

The first layer coated with medronic acid will generate phosphate bridges, functioning as a corrosion-resistant sheath layer, and will be the only connector to Forteo (Teriparatide Acetate). The second layer encloses the essential elements of teriparatide like C, N, O and H with saving the functional radicals like CNO<sup>•</sup>, C<sub>2</sub>H<sub>3</sub>O<sup>•</sup>, CHO<sub>2</sub><sup>•</sup>, C<sub>3</sub>H<sub>3</sub>O<sup>•</sup>, C<sub>2</sub>H<sub>3</sub>O<sub>2</sub><sup>•</sup>, for and it will stimulate the coated implant fixture with PTH receptors, osteoblasts, and osteogenesis. The first layer covers Ti-O-P, acting as a titanium grade 4 antioxidant.

#### Conclusion

The top surface ions in the second layer of the fixture have pharmaceutically functioning parts of the chemical structure of Teriparatide (C<sub>181</sub>H<sub>291</sub>N<sub>55</sub>O<sub>51</sub>S<sub>2</sub>) activating osteoblasts more than osteoclasts, which leads to an overall increase in bone. Though the recommended duration of use for grade 4 implant fixtures is 3 years, but these new coated fixtures are expected to use the coated fixtures longer than 3 years by containing the stimulating effect of new alveolar bone formation by increasing the mineral density of the alveolar bone around the fixture besides preventing corrosional toxicity of the surface of preexisting titanium fixtures.

**Keywords:** Carcinogens, Titanium, Oxidation-Reduction, Hypersensitivity, Phosphates, Teriparatide

Date of Submission: 04-08-2021

Date of acceptance: 17-08-2021

## I. INTRODUCTION

As the 30-years used dental fixture, titanium dioxide is a public carcinogen classified as a member of Group 2B by the International Agency for Research on Cancer (IARC). It is easily oxidized and corroded by saliva, fluoride in toothpaste, acidic foods, and hot soup. Partial exposures of the fixture due to the retraction of the gums

and alveolar bone increase the chance of contact with the bolus, body fluids and air, accelerating the oxidation and corrosion reactions. Titanium dioxide particles are found in nearby alveolar bones, oral lymph nodes, and lungs. Their harm includes genetic damage, carcinogenic, yellow nail syndrome, graft failure, inhibition of apatite formation and allergic contact dermatitis [1,2]. In plasma, urine, and exhaled condensate, a case of dermatological allergy appeared in physiological problems in markers of oxidative stress and inflammation [3], and osteoporosis in the vicinity of the fixture implanted in the patient's alveolar bone [4].

A normal dental implant fixture should not cause these allergic reactions or osteoporosis in the patient after placement. Moreover, it must be replaced with a material that can avoid oxidation and corrosion that cause such reactions, and it must also have the function of inducing osseointegration that conventional titanium had. Hence, the ideal dental implant is to replace titanium by coating the surface with Teriparatide, a treating agent of osteoporosis that causes osseointegration while maintaining the rigidity of titanium.

**II. MATERIALS**

Two implant fixtures were fabricated in grade 4 (pure titanium) from Angels and Trausim with 99% purity. The suppliers are Trausim Medical Devices Co., Ltd. in Jiangsu Province, China, and Foshan Angels Biotechnology Co., Ltd, located in Foshan, China. Medronic (methylene diphosphonic) acid (MDP;  $\text{CH}_6\text{O}_6\text{P}_2$ ) of 100% purity is manufactured by Apollo Scientific Ltd. (Stockport, UK), and Teriparatide is produced by Teriparatide Injection, 600mcg, Lilly Korea Ltd, South Korea.

Teriparatide liquid is contained in two plastic Eppendorf microtubes, and dental UV radiated to them after entering two dental fixtures Angels and Trausim immersed in Teriparatide (wavelength range: 420nm to 490nm, Prolux 770-I LED Curing Light, Taiwan Peng Lim) confirmed the results of SEM (Scanning Electron Microscope), EDS (Energy Dispersion Spectrometry), XPS (X-ray Photoelectron Spectroscopy) and Tof-SIMS (Time-of-Flight Secondary Ion Mass Spectroscopy).

**Double coating system**

**Goals and objectives**

The primary purpose of these two layers is to prevent corrosion of the surface of the titanium fixture beneath the first layer, after coating with Medronic acid to form phosphate bridges, and the secondly coated Teriparatide layer will induce the implant osseointegration of the implant (Fig 1) [5].

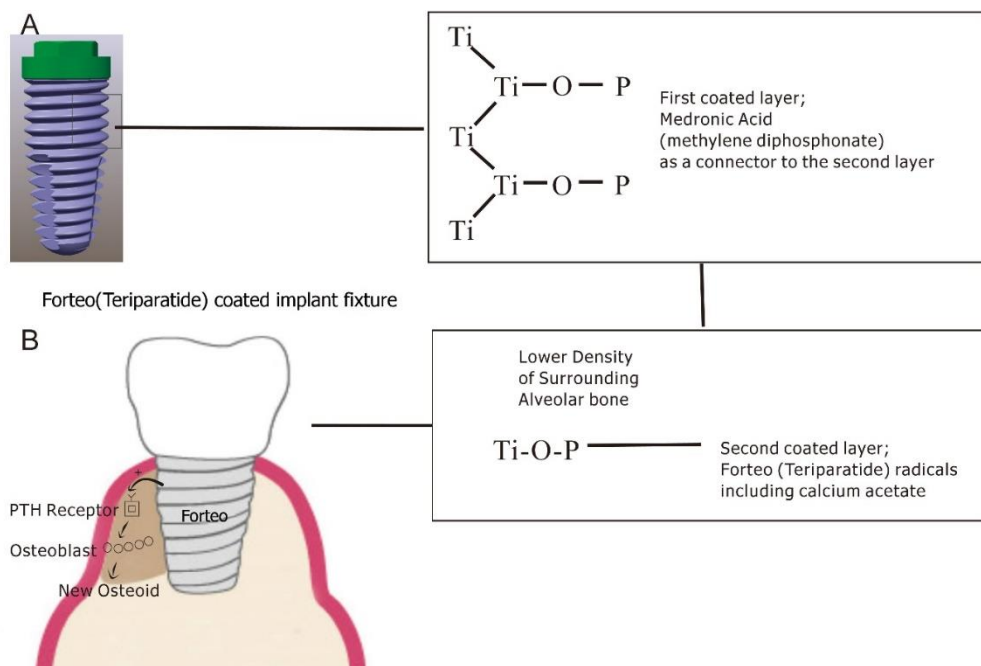


**Fig. 1.** Schematic structure of a double coating system for preventing  $\text{TiO}_2$  corrosion in a dental implant fixture. (A) First coated layer of Ti-O-P link to prevent Ti-O<sub>2</sub> corrosion. (B) Mechanism of coated Teriparatide (Forteo)-stimulated osteoblast coating.

Surface modification with medronic (methylenediphosphonic) acid (MDP) was demonstrated by grafting on a polished Ti grade 4 fixture and was obtained via chemical adsorption from MDP solution for one day at room temperature under the following conditions: MDP,  $1.5 \times 10^{-3}$  M in 10 mL of double distilled water. After grafting, the fixture was rinsed with double distilled water to remove physically absorbed phosphonic acid, dried in vacuum (1333 Pa, RT) and analyzed by SEM, XPS and ToF-SIMS. This result of XPS after one layer coating showed that P-O-Ti bonds were formed on the surface.

#### First layer

Medronic acid was diluted with distilled water in a ratio of 1:4 and the two fixtures were immersed in two plastic Eppendorf tubes for a day at room temperature and pulled out to perform SEM, EDS, XPS and ToF-SIMS tests.

#### Second layer

In the alveolar bone near the dental implant fixture, if the portion of the alveolar bone near the expected implant is low density, Teriparatide Acetate (Forteo) coating can be applied with UV (Ultra Violet) rays in the range of about 100-400nm. The conjugated double bonds of the benzene ring peak mainly at 180 and 200 nm. Below 200nm, it should be used in a vacuum chamber to prevent unwanted UV absorption by air. UV rays at 250 or 350 nm are often used to open the benzene ring [6]. The aromatic ring consists of a pi bond that absorbs ultraviolet rays. The pi electrons in the ring absorb ultraviolet rays and are stabilized by the surrounding ring. In Forteo, there is a functional aromatic ring called 'imidazole ring' that stimulates osteoclasts such as Zoledronic acid [7,8,9]. We use UV to break this ring and reuse the blocked chemical bonds in this ring as a bridge for no need to stimulate osteoclasts. And other parts of Forteo that receive UV light still contain the pharmaceutical function of stimulating osteoblasts to form alveolar bone near the fixture.

The two nitrogen atoms of this imidazole ring can accept and release cations, and since this imidazole's functional group pKa is close to 7, it is possible to regulate the dissociation of  $H^+$  with slight changes in the human body in the neutral state of pH[10]. The nitrogen cations of imidazole can easily release cations and catch unwanted electrons released from oxidation of pure titanium by UV. The nano-sized anatase  $TiO_2$  does not absorb visible light, but strongly absorbs ultraviolet (UV) radiation (hv) to form hydroxyl radicals.

Through sinking in medronic acid, Ti-O-P-O<sub>2</sub> bonds were formed on the surface of the titanium implant fixture. The Teriparatide liquid is contained in two plastic Eppendorf microtubes and two dental fixtures of Angels and Trausim was inputted on sinking in Teriparatide liquid and then a dental UV (wavelength range: 420nm to 490nm, Prolux) by 770-I LED Curing Light (Peng Lim, Taiwan) was emitted to confirm the results of SEM, EDS, XPS and ToF-SIMS.

#### XPS (X-ray photoelectron spectroscopy)

In X-ray photoelectron spectroscopy (XPS) named ESCA (electron spectroscopy for chemical analysis), a characteristic of X-ray (monochromatic X-ray source) is an incident on the surface of a sample in an ultra-high vacuum chamber, and the energy of the photoelectrons is at the atomic level (1,000-1,500). By measuring eV, we can obtain information on the elemental composition and chemical bonding state of the sample surface [11]. It can be applied to non-conductive insulators using a flood gun that performs charge neutralization [12,13], so the surface can be etched with an Ar ion beam to measure its distribution over depth [14,15,16,17].

For all samples, the analysis results are expressed in atomic % [18]. Since this technique obtains the qualitative and quantitative composition of the outermost layer of the material (for metals, the analyzed depth is about 5 nm), it directly displays the chemical composition of the layer of fixture in contact with the alveolar tissue effectively.

The XPS analysis was performed with K-Alpha+ manufactured by Thermo-Fisher Scientific, the X-Ray spot size is 30 to 400  $\mu m$  in 5  $\mu m$  steps, and the energy resolution is less than 0.5 eV FWHM (full width up to half). It is equipped with a monochromatic X-ray source with an Al anode maintained at 20kV with a power of 200W. The analyzed depth is about 5 nm with an area of about 300  $\mu m$  in diameter. The pressure inside the analysis chamber was maintained at about  $10^{-9}$  Torr. XPS spectra were acquired with the same instrument using a non-monochromatic source with an Mg anode.

In Table 1, the composition of the surface was analyzed using X-ray Photoelectron Spectroscopy (XPS) on two dental implant fixtures carved by Angels and Trausim. The analysis mode is surface and the Ar etch and x-ray source is 200  $\mu m$ . The composition of the two implant fixtures is C, Ca, Na, O, Si, Ti, and Zn.

	C1s	Ca2p	Na1s	O1s	Si2p	Ti2p	Zn2p
ANGELS	81.83	1.25	0.33	13.3	2.09	1.07	0.14
ANGELS_etch	68.2	1.4	0.97	19.98	1.24	8.22	0
TRAUSIM	80.4	0.35	1.4	13.49	2.36	1.1	0.89
TRAUSIM_etch	74.85	0.97	1.47	15.3	1.38	5.34	0.69

**Table 1.** Surface composition [unit: At (Ampere-Turn). %]

Carbon dioxide is known as a chemically inert gas and reacts with many metal oxides and hydroxides to form carbonates. This air-carbon gas easily adhered to the  $\text{TiO}_2$  surface of fixtures by its excessive activity after the titanium has been oxidized [19, 20]. Conversely, nitrogen, which exists in a diatomic state, contains triple bonds and does not react at room temperature because it dissociates slightly even when heated above 3000 °C. O1s refers to the deep oxidation that proceeds to the first orbit of oxygen, and human contact reveals small amounts of Ca, Na, and Zn originating from sweat on the fingers touching the fixtures. Both samples in Table 1 are Ar etched at 1 keV for 30 seconds and etched about 7-10 nm. For the Si2p (Silicon 2p orbital) peak scan, a binding energy of about 110 eV was marked as a peak, which is evidence of the presence of Silicon contamination as Silicon is the second most abundant element in the sun and stars, making up over a quarter of the earth's crust. Before etching, the amount of Ti on the fixture surface was 1.07 and 1.1 for Angels and Trausim, but these numbers increased to 8.22 and 5.34, respectively. Conversely, other elements such as C, Si, and Zn showed reduced amounts after etching, and it can be confirmed that these elements adhere to the surface area by contamination and can be removed by etching techniques.

Secondary XPS results show chemical shift by coated phosphate. New phosphate peaks were recorded in both fixtures. This strength is related to the number of phosphate atoms with their respective oxidation states, including  $-\text{PO}_2^-$  and  $-\text{PO}_3^-$ . When the coated phosphate atoms diffuse to the fixture surface, the XPS strength increases.

The 3rd XPS results are newly observed on the surface of the two fixtures after coating of the main elements of teriparatide, C and the second main elements N and O (**Fig 2**).

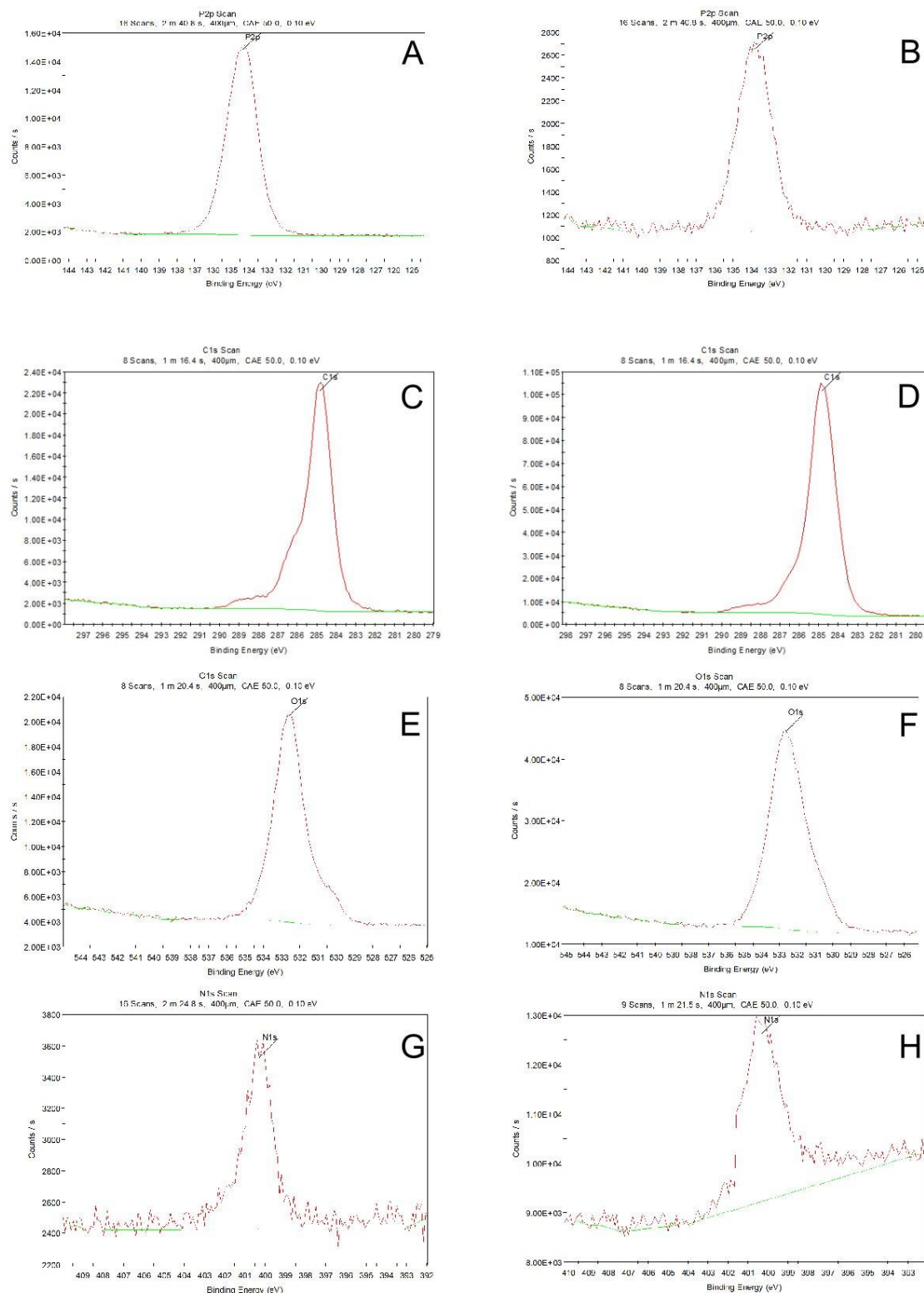


**Fig 2. A, B, C, D, E, F, G and H** XPS Peaks of Angel's (A, C, E and G) and Trausim's (B, D, F and H), Every binding energy of P, C, O, and N is plotted.

### EDS (Energy Dispersion Spectroscopy)

As an energy dispersive spectrometer, the EDS electron gun was a Schottky field emitter. The energy dissipation peak of phosphate was newly strengthened in both fixtures. The EDS spectrum of the coated fixture of medronic acid showed a surface similar to the C and O peaks. Conversely, the Ti peak is located at the bottom of the EDS, which means a weak energy dissipation screened by the P peak in the outer layer.

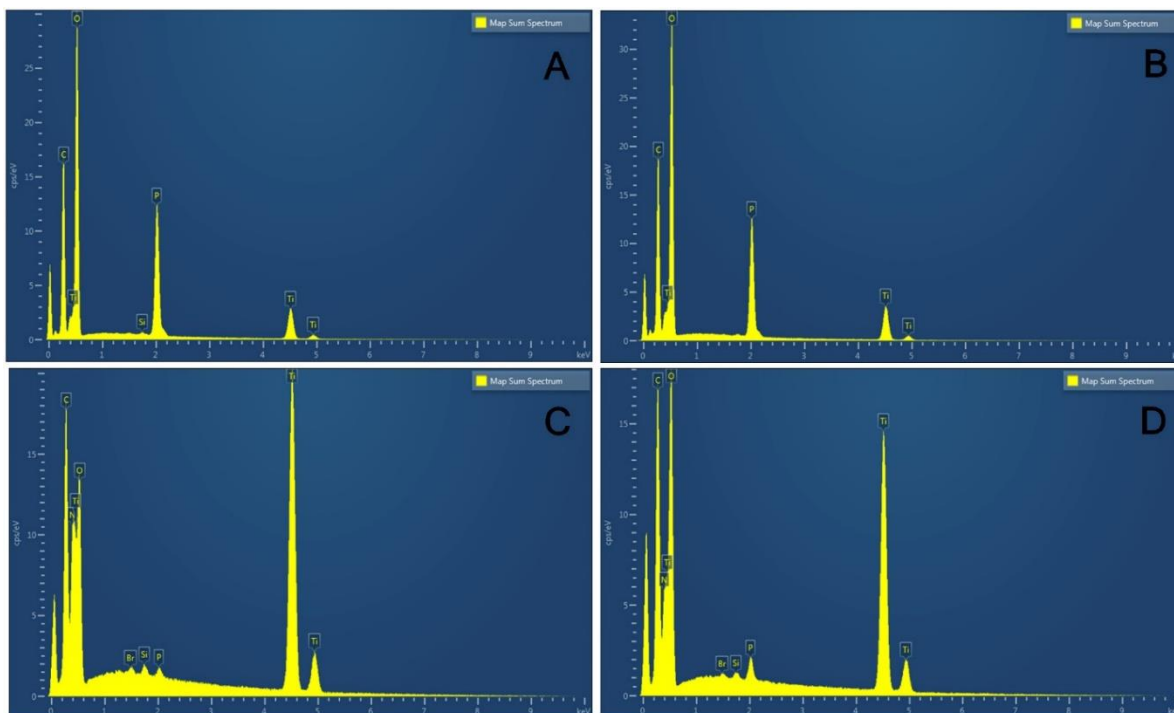


**Fig 3.A, B, C and D** Comparison of Medronic acid coating and Teriparatide coatings by EDS graphs (A and C: Angels, B and D: Trausim); After coating Angels with medronic acid (A), after coating with medronic acid on Trausim (B). In contrast, after Teriparatide coating, the main element of C and the second main elements N, O, show the strongest energy peaks after coating (C and D).

### SEM (scanning electron microscope)

#### Device

ZEISS Merlin® FE-SEM was used for microscopic analysis of the fixture surface. FE (Computerized Field Emission)-Scanning Electron Microscope (SEM) with patented GEMINI II electromagnetic/electrostatic objective lens system. Resolution SEM has 0.8 nm @ 15 kV, 1.4 nm @ 1 kV, acceleration voltage: 0,02-30 kV, and Schottky field emitters.

The X-ray and UV photoelectron spectrometer for XPS analysis is K-alpha+ from Thermo Fisher Scientific in Waltham, MA, with a minimum energy step size of 3 meV and an ultimate energy resolution of less than 0.5 eV for the Ag 3d 5/2 peak. FWHM, ultimate spatial resolution is less than 30µm by Knife Edge method, XPS in 1s energy resolution (eV) of C insulator is less than 0.85eV, passing energy is 1-400eV.

#### Secondary electron (SE)

Secondary electrons occur on the surface or near the surface of the sample [21]. These are the result of inelastic interactions between the primary electron beam and the sample and have lower energy than backscattered electrons [22]. Secondary electrons are very useful for examining the topography of a sample surface [23]. They consist of scintillators inside a Faraday cage that carries a positive charge and attracts the SE. Scintillators inside the Faraday cage are positively charged enough to attract the SE, and are used to accelerate and convert secondary electrons into light before reaching the photomultiplier for amplification [24]. These two types of electrons are the most used signals for imaging by SEM users.

Topographic evaluation was evaluated using a scanning electron microscope (SEM) and a diffuse inverse electron detector (BSE = backscatter electrons) in normal mode. Observations were made using a Merlin Computerized Field Emission (FE)-SEM (Scanning Electron Microscope) instrument (ZEISS). The main parameters of the analysis are electron = HV, working distance = WD, detector type = signal, magnification = Mag, and acceleration high voltage for Kelvin probe force microscope = KFM. KFM for electrical resistance evaluation-as a work function in the outdoor/vacuum environment mode, the work function of the surface shown directly in the photo is measured with a microscope. SEM analysis, performed using a detector capable of detecting backscattered electrons (BSE), is due to the fact that the backscattering efficiency is a function of the atomic number [25,26]. Contaminants of different chemical nature are easily visualized thanks to the shades of gray that are created by these BSE.

In particular, using the principle of stereoscopic vision, two representative images of the terrain were obtained with two slightly different viewing angles for Angels and Trausim, i.e., with the specimen holder slightly inclined (tilt angle). Using an inclination angle of 25 degrees, images were obtained at 260x, 300x, 500x and 2000x, the areas analyzed in KFM were  $200 \times 200$ ,  $400 \times 400$  and  $900 \times 900 \mu\text{m}^2$ , and the geometrical areas evaluated were 40,000, 160,000 and 180,000  $\mu\text{m}^2$ .

Conventional dental implant fixtures easily show unwanted oxidation as shown in the SEM image below. The whitened parts of the fixture are the oxidized in titanium grade 4 (commercially pure titanium). Various magnifications are applied from 1mm to 20, 50, 100, 200 and 300 $\mu\text{m}$ . The agglomerated white  $\text{TiO}_2$  particles were found in micrometer size, and the average size of the agglomerated and white oxide particles was less than about 20 nm.

In SEM, the two types of electrons are mainly detected as backscattered electrons (BSE) and secondary electrons (SE). Backscattered electrons are reflected back after the elastic interaction between the beam and the sample [27]. However, secondary electrons come from atoms in the sample. This is the result of the inelastic interaction between the electron beam and the sample.

BSE comes from a deeper area of the sample but SE occurs in the surface area. Thus, BSE and SE carry different types of information. BSE images show high sensitivity to differences in atomic number [28]. The higher the atomic number, the brighter the material will appear in the image. SE imaging can provide more detailed surface information [29].

We used SE mode to check if the coated surface area still revealed the oxidized surface of Ti. Both fixtures were gold sputtered and the implant surface was analyzed using SEM and EDS to investigate the formation of an apatite-like layer on the implant surface. The working distance is from 10.0mm to 9.2mm in the BSE (back scattered electrons) mode.

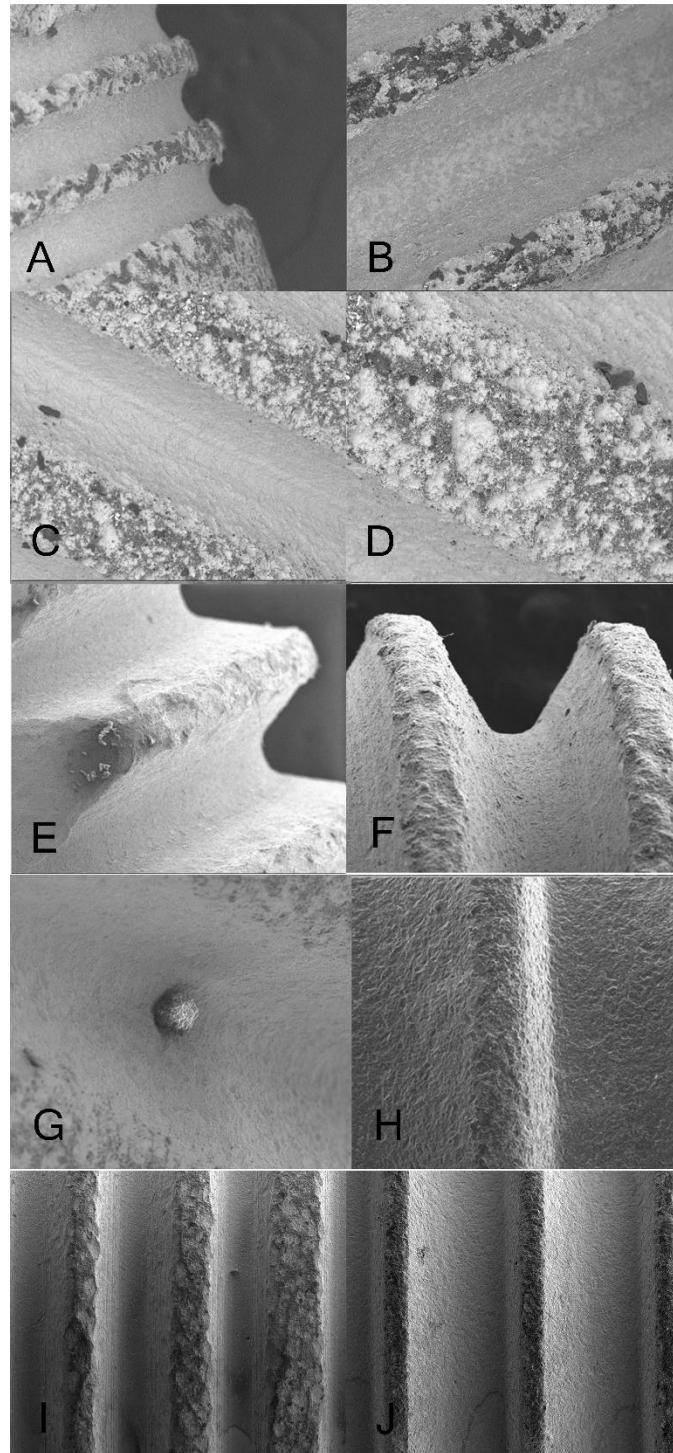


**Fig 4.** SEM images

**A and B** The white oxide particles of  $\text{TiO}_2$  are more clearly visible in the thread than in the groove SEM images of the surface of the implant fixture manufactured by Trausim. Inc. **C and D** The center of the thread is more agglomerated than the edges and shows larger white chunks, still showing small, unoxidized black areas between the white chunks. **E, F, G and H** The surface is protected from further oxidation as after phosphate coating, and no special white oxide agglomerates that collected more electrons after Ti oxidation on the fixture surface. Before (E and G) and after (F and H) the Medronic acid coating, the white oxide particles of  $\text{TiO}_2$  disappeared. Trausim. **I and J** Comparison of Teriparatide Coating by SEM Image. (I) is Angel and (J) is Trausim.

### Tof-SIMS (Time-of-Flight Secondary Ion Mass Spectroscopy)

Secondary ion mass spectrometry (SIMS) is at IONTOF GmbH, TOF-SIMS 5 in Münster, Germany, with a mass range of 0-10,000 amu, a mass resolution of less than 10000, a spatial resolution of less than 300 nm, and a beam energy of 25. kV Bi +, 10 kV Cs + and C60+.

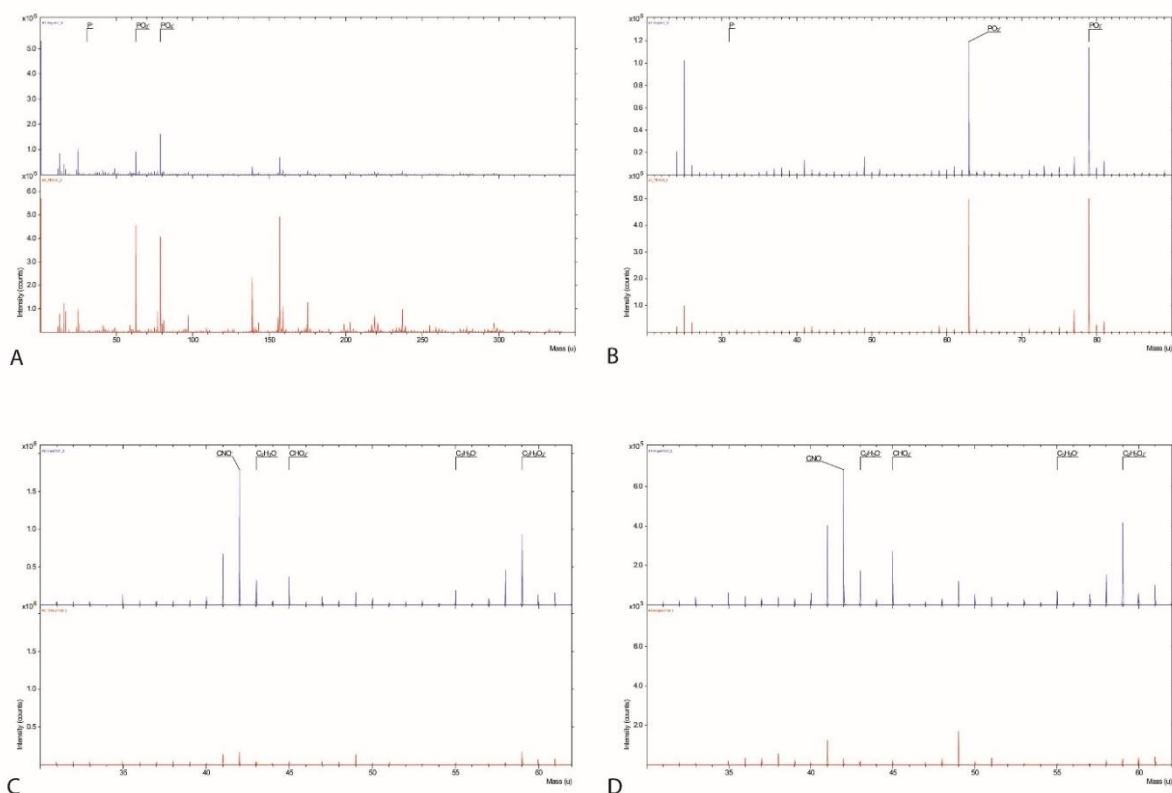


Fig 5. Tof-SIMS

**A and B** Using a pulsed ion beam, Tof-SIMS detects the flight time of this mass and molecular ion with a mass to charge ratio of 1 to 10,000 m/z mass/zahl (number of electron charges) [30,31]. This single spectrum provides surface information of solid materials for chemical elements, states, and molecular information [32,33,34]. In the surface spectrum, P<sup>-</sup>, PO<sub>2</sub><sup>-</sup>, and PO<sub>3</sub><sup>-</sup> peaks are detected on the surface of #1-Angels (A) & #2-Trausim (B), and P compounds are detected as main components on the surface of both samples after the first layer coating of medronic acid. **C and D** However, CNO compounds such as the secondary surface spectrum, CNO<sup>-</sup>, C<sub>2</sub>H<sub>3</sub>O<sup>-</sup>, CHO<sub>2</sub><sup>-</sup>, C<sub>3</sub>H<sub>3</sub>O<sup>-</sup>, C<sub>2</sub>H<sub>3</sub>O<sub>2</sub><sup>-</sup>, are detected in the same samples after the secondary coating of teriparatide. Each spectrum shares the same surface analysis parameters. PI: Bi3 energy is 30keV, analysis area is 100×00 μm<sup>2</sup>, target current is 0.7-0.8pA, polarity is positive and negative.

### III. RESULTS AND CONCLUSION

We expect the first layer coated with medronic acid will generate phosphate bridges, functioning as a corrosion-resistant sheath layer, and will be the only connector to Forteo (Teriparatide Acetate). The second layer encloses the essential elements of teriparatide like C, N, O and H with saving the functional radicals like CNO<sup>-</sup>, C<sub>2</sub>H<sub>3</sub>O<sup>-</sup>, CHO<sub>2</sub><sup>-</sup>, C<sub>3</sub>H<sub>3</sub>O<sup>-</sup>, C<sub>2</sub>H<sub>3</sub>O<sub>2</sub><sup>-</sup>, and it will stimulate the coated implant fixture with PTH receptors, osteoblasts, and osteogenesis. The first layer covers Ti-O-P, acting as a titanium grade 4 antioxidant.

The color of the first coated layer is not the same as the second layer with the naked eye. This colorful difference in SEM analysis is achieved by removing the white spots caused by oxidation. Our interest is to observe the correlation between color and surface adhesion composition of elements other than TiO<sub>2</sub>.

The top surface ions in the second layer of the fixture such as CNO compounds, CNO<sup>-</sup>, C<sub>2</sub>H<sub>3</sub>O<sup>-</sup>, CHO<sub>2</sub><sup>-</sup>, C<sub>3</sub>H<sub>3</sub>O<sup>-</sup> and C<sub>2</sub>H<sub>3</sub>O<sub>2</sub><sup>-</sup> and C<sub>2</sub>H<sub>3</sub>O<sub>2</sub><sup>-</sup> are essential functional radicals by peptide fragments of Teriparatide. These

parts of the chemical structure of Teriparatide ( $C_{181}H_{291}N_{55}O_{51}S_2$ ) activate osteoblasts more than osteoclasts, which leads to an overall increase in bone. The recommended duration of use for grade 4 implant fixtures is 3 years, and these new coated fixtures are expected to contain the stimulating effect of new alveolar bone formation by increasing the mineral density of the alveolar bone around the fixture.

Further research will focus on the ability of the newly coated fixture to prevent allergic reactions and alveolar bone loss after implantation, and to confirm an unknown relationship with the color of the coated layer.

### Conflict of Interest

“The author(s) declare(s) that there is no conflict of interests regarding the publication of this article”.

### REFERENCES

- [1]. N. Schiff, B. Grosgeat, M. Lissac, F. Dalard, Influence of fluoridated mouthwashes on corrosion resistance of orthodontics wires, *Biomaterials* 25(19) (2004) 4535-42.
- [2]. S. Vignes, R. Baran, Yellow nail syndrome: a review, *Orphanet J Rare Dis* 12(1) (2017) 42.
- [3]. M. Hosoki, K. Nishigawa, Y. Miyamoto, G. Ohe, Y. Matsuka, Allergic contact dermatitis caused by titanium screws and dental implants, *J Prosthodont Res* 60(3) (2016) 213-9.
- [4]. L.A. du Preez, K.W. Butow, T.J. Swart, Implant failure due to titanium hypersensitivity/allergy?--Report of a case, *SADJ* 62(1) (2007) 22, 24-5.
- [5]. U. Kuchler, E.R. Luvizuto, S. Tangl, G. Watzek, R. Gruber, Short-term teriparatide delivery and osseointegration: a clinical feasibility study, *J Dent Res* 90(8) (2011) 1001-6.
- [6]. S. Nikafshar, O. Zabihi, M. Ahmadi, A. Mirmohseni, M. Taseidifar, M. Naebe, The Effects of UV Light on the Chemical and Mechanical Properties of a Transparent Epoxy-Diamine System in the Presence of an Organic UV Absorber, *Materials (Basel)* 10(2) (2017) 180.
- [7]. H.J. Ihn, T. Lee, D. Lee, J.S. Bae, S.H. Kim, I.H. Jang, Y.C. Bae, H.I. Shin, E.K. Park, Inhibitory Effect of KP-A038 on Osteoclastogenesis and Inflammatory Bone Loss Is Associated With Downregulation of Blimp1, *Front Pharmacol* 10 (2019) 367.
- [8]. J. Lin, Y. Peng, Q. Liu, K. Li, G. Lv, Y. Seimbille, G. Huang, F. Gao, L. Qiu, Pharmacological evaluation of imidazole-derived bisphosphonates on receptor activator of nuclear factor-kappaB ligand-induced osteoclast differentiation and function, *Chem Biol Drug Des* 97(1) (2021) 121-133.
- [9]. L. Wang, D. Fang, J. Xu, R. Luo, Various pathways of zoledronic acid against osteoclasts and bone cancer metastasis: a brief review, *BMC Cancer* 20(1) (2020) 1059.
- [10]. I.M.A. Omar, A.M. Al-Fakih, M. Aziz, K.M. Emran, Part II: Impact of ionic liquids as anticorrosives and additives on Ni-Co alloy electrodeposition: Experimental and DFT study, *Arabian Journal of Chemistry* 14(1) (2021) 102909.
- [11]. C.R. Brundle, B.V. Crist, X-ray photoelectron spectroscopy: A perspective on quantitation accuracy for composition analysis of homogeneous materials, *Journal of Vacuum Science & Technology A* 38(4) (2020) 041001.
- [12]. D.R. Baer, M.H. Engelhard, D.J. Gaspar, A.S. Lea, C.F. Windisch Jr, Use and limitations of electron flood gun control of surface potential during XPS: two non-homogeneous sample types, *Surface and Interface Analysis* 33(10-11) (2002) 781-790.
- [13]. L. Edwards, P. Mack, D.J. Morgan, Recent advances in dual mode charge compensation for XPS analysis, *Surface and Interface Analysis* 51(9) (2019) 925-933.
- [14]. N. Savvides, Surface microroughness of ion-beam etched optical surfaces, *Journal of Applied Physics* 97(5) (2005) 053517.
- [15]. S. Yoshimura, K. Ikuse, Y. Tsukazaki, M. Kiuchi, S. Hamaguchi, Effect of ultraviolet light irradiation on etching process of poly(methyl methacrylate) by ion beam injections, *Journal of Physics: Conference Series* 191 (2009) 012030.
- [16]. J.W. Park, D.S. Kim, W.O. Lee, J.E. Kim, G.Y. Yeom, Atomic layer etching of chrome using ion beams, *Nanotechnology* 30(8) (2018) 085303.
- [17]. Y. Zhong, Y. Dai, F. Shi, C. Song, Y. Tian, Z. Lin, W. Zhang, Y. Shen, Effects of Ion Beam Etching on the Nanoscale Damage Precursor Evolution of Fused Silica, *Materials* 13(6) (2020) 1294.
- [18]. G. Zorn, S.R. Dave, X. Gao, D.G. Castner, Method for Determining the Elemental Composition and Distribution in Semiconductor Core-Shell Quantum Dots, *Analytical Chemistry* 83(3) (2011) 866-873.
- [19]. S. Al Jitan, G. Palmisano, C. Garlisi, Synthesis and Surface Modification of TiO<sub>2</sub>-Based Photocatalysts for the Conversion of CO<sub>2</sub>, *Catalysts* 10(2) (2020) 227.
- [20]. T.P. Nguyen, D.L.T. Nguyen, V.H. Nguyen, T.H. Le, D.N. Vo, Q.T. Trinh, S.R. Bae, S.Y. Chae, S.Y. Kim, Q.V. Le, Recent Advances in TiO<sub>2</sub>-Based Photocatalysts for Reduction of CO<sub>2</sub> to Fuels, *Nanomaterials (Basel)* 10(2) (2020).
- [21]. D. Bajek, S. Wackerow, D.A. Zanin, L. Baudin, K. Bogdanowicz, E.G. Valdivieso, S. Calatroni, B. Di Girolamo, M. Sitko, M. Himmerlich, M. Taborelli, P. Chiggiato, A. Abdolvand, Role of surface microgeometries on electron escape probability and secondary electron yield of metal surfaces, *Sci Rep* 10(1) (2020) 250.
- [22]. M.T. Postek, A.E. Vladar, J.S. Villarrubia, A. Muto, Comparison of Electron Imaging Modes for Dimensional Measurements in the Scanning Electron Microscope, *Microsc Microanal* 22(4) (2016) 768-77.
- [23]. F.A. Shah, K. Ruscsak, A. Palmquist, 50 years of scanning electron microscopy of bone-a comprehensive overview of the important discoveries made and insights gained into bone material properties in health, disease, and taphonomy, *Bone Res* 7 (2019) 15.
- [24]. S. Polyakov, Chapter 3@ Photomultiplier Tubes, *Experimental Methods in The Physical Sciences* 45 (2013) 69-82.
- [25]. A. Bentabet, N.E. Fenineche, Backscattering coefficients for low energy electrons and positrons impinging on metallic thin films: scaling study, *Applied Physics A* 97(2) (2009) 425.
- [26]. R. Skoupy, T. Fort, V. Krzyzanek, Nanoscale Estimation of Coating Thickness on Substrates via Standardless BSE Detector Calibration, *Nanomaterials* 10(2) (2020) 332.
- [27]. E.A. Jackson, Y. Wu, W.J. Frost, J.-Y. Kim, M. Samiepour, K. Elphick, M. Sun, T. Kubota, K. Takahashi, T. Ichinose, S. Mizukami, A. Hirohata, Non-destructive imaging for quality assurance of magnetoresistive random-access memory junctions, *Journal of Physics D: Applied Physics* 53 (2019).

- [28]. K.H. Kim, Z. Akase, T. Suzuki, D. Shindo, Charging Effects on SEM/SIM Contrast of Metal/Insulator System in Various Metallic Coating Conditions, *MATERIALS TRANSACTIONS* 51(6) (2010) 1080-1083.
- [29]. W.-R. Lin, Y.-J. Chuang, C.-H. Lee, F.-G. Tseng, F.-R. Chen, Fabrication and Characterization of a High-Performance Multi-Annular Backscattered Electron Detector for Desktop SEM, *Sensors* 18(9) (2018) 3093.
- [30]. A.V. Ievlev, A. Belianinov, S. Jesse, D.P. Allison, M.J. Doktycz, S.T. Retterer, S.V. Kalinin, O.S. Ovchinnikova, Automated Interpretation and Extraction of Topographic Information from Time of Flight Secondary Ion Mass Spectrometry Data, *Scientific Reports* 7(1) (2017) 17099.
- [31]. J. Jiang, L. Hua, Y. Xie, Y. Cao, Y. Wen, P. Chen, H. Li, High Mass Resolution Multireflection Time-of-Flight Secondary Ion Mass Spectrometer, *Journal of the American Society for Mass Spectrometry* 32(5) (2021) 1196-1204.
- [32]. S. Mourdikoudis, R.M. Pallares, N.T.K. Thanh, Characterization techniques for nanoparticles: comparison and complementarity upon studying nanoparticle properties, *Nanoscale* 10(27) (2018) 12871-12934.
- [33]. S. Sharma, S. Jaiswal, B. Duffy, A.K. Jaiswal, Nanostructured Materials for Food Applications: Spectroscopy, Microscopy and Physical Properties, *Bioengineering (Basel)* 6(1) (2019) 26.
- [34]. Y. Chen, R.W. Dorn, M.P. Hanrahan, L. Wei, R. Blome-Fernández, A.M. Medina-Gonzalez, M.A.S. Adamson, A.H. Flintgruber, J. Vela, A.J. Rossini, Revealing the Surface Structure of CdSe Nanocrystals by Dynamic Nuclear Polarization-Enhanced <sup>77</sup>Se and <sup>113</sup>Cd Solid-State NMR Spectroscopy, *Journal of the American Chemical Society* 143(23) (2021) 8747-8760.

#### \*text-only\* main figure/table legend

**[Pic 1]** Schematic structure of a double coating system for preventing TiO<sub>2</sub> corrosion in a dental implant fixture. (A) First coated layer of Ti-O-P link to prevent Ti-O<sub>2</sub> corrosion. (B) Mechanism of coated Teriparatide (Forteo)-stimulated osteoblast coating.

**[Pic 2]** Peaks of Angel's XPS (left) and Trausim (right), The binding energy of P, C, O, and N (left is Angel, right is Trausim)

**[Pic 3]** Comparison of Teriparatide coating by EDS graph (Left: Angel, Right: Trausim); After coating angels with medronic acid (left), after coating with medronic acid on Trausim (right), Teriparatide, the main element of C and the second main elements N, O, show the strongest energy peaks after coating

#### **[Pic 4] SEM images**

The white oxide particles of TiO<sub>2</sub> are more clearly visible in the thread than in the groove **[Pic 4: A and B]**. SEM image of the surface of the implant fixture manufactured by Trausim. Inc. The center of the thread is more agglomerated than the edges and shows larger white chunks, still showing small, unoxidized black areas between the white chunks **[Pic 4: C and D]**. The surface is protected from further oxidation as after phosphate coating, and no special white oxide agglomerates that collected more electrons after Ti oxidation on the fixture surface. Before and after the medronic acid coating, the white oxide particles of TiO<sub>2</sub> disappeared. Trausim: Before Medronic Acid Coating (Left) and After Medronic Acid Coating (Right) **[Pic 4: E, F, G and H]**. Comparison of Teriparatide Coating by SEM Image (Left: Angel, Right: Trausim) **[Pic 4: I and J]**

#### **[Pic 5] Tof-SIMS**

Using a pulsed ion beam, Tof-SIMS detects the flight time of this mass and molecular ion with a mass to charge ratio of 1 to 10,000 m/z mass/zahl (number of electron charges) (Ievlev et al., 2017; Jiang et al., 2021). This single spectrum provides surface information of solid materials for chemical elements, states, and molecular information (Mourdikoudis et al., 2018; Sharma et al., 2019; Chen et al., 2021). In the surface spectrum, P<sup>-</sup>, PO<sub>2</sub><sup>-</sup>, and PO<sub>3</sub><sup>-</sup> peaks are detected on the surface of #1-Angels (left) & #2-Trausim (right), and P compounds are detected as main components on the surface of both samples after the first layer coating of medronic acid **[Pic 5: A and B]**. However, CNO compounds such as the secondary surface spectrum, CNO<sup>-</sup>, C<sub>2</sub>H<sub>3</sub>O<sup>-</sup>, CHO<sub>2</sub><sup>-</sup>, C<sub>3</sub>H<sub>3</sub>O<sup>-</sup>, C<sub>2</sub>H<sub>3</sub>O<sub>2</sub><sup>-</sup>, are detected in the same samples after the secondary coating of teriparatide. Each spectrum shares the same surface analysis parameters. PI: Bi3 energy is 30keV, analysis area is 100×00 μm<sup>2</sup>, target current is 0.7-0.8pA, polarity is positive and negative **[Pic 5: C and D]**.

#### Appendix

	C1s	Ca2p	Na1s	O1s	Si2p	Ti2p	Zn2p
ANGELS	81.83	1.25	0.33	13.3	2.09	1.07	0.14
ANGELS_etch	68.2	1.4	0.97	19.98	1.24	8.22	0
TRAUSIM	80.4	0.35	1.4	13.49	2.36	1.1	0.89
TRAUSIM_etch	74.85	0.97	1.47	15.3	1.38	5.34	0.69

**[Table 1]** Surface composition [Unit: At (Ampere-Turn)). %]